Current Science
CS 5 (3), 2141-2149 (2025)
Received 13 Feb 2025 | **Revised 12 March** 2025 | **Accepted 13April**. 2025 | **Online Available 4 May** 2025
https://doi.org/ 10.52845/CS/2025-5-3-8

Current Science

Current Science

OPEN ACCESS

ISSN(O)2795-8639

Orignal Article

Age-Stratified Glycolysis and Bile Acid Metabolism Drive Survival in Acute Liver Failure: Insights from NCBI Pathways

Xiuwen Wang[1]*[#], Yicun Wang2[#], Ping Zhao[1]

[1]College of Life Sciences, Jilin Normal University, No. 1301, Hai Feng Street, Tiexi District, Siping City, 136000, China

[2]Department of Medical Research Center, Second Hospital of Jilin University, Chang Chun, 130041, PR China

[*]Corresponding Author: Xiuwen Wang

Abstract:

Objective: This study investigates age-dependent variations in hepatic glycolytic adaptation during D-galactosamine-induced acute liver failure (ALF), identifying metabolic regulators through integrated bioinformatics analyses leveraging NCBI-annotated datasets.

Methods: Age-stratified male Wistar rats (6-week juvenile vs 8-month middle-aged) received D-GalN (YDI/MDI) or PBS. Multi-omics analysis combining hepatic transcriptomics, serum enzyme analyses, and qPCR validation was conducted at 24h post-challenge. Multi-omics pathway analysis incorporated NCBI GEO/KEGG resources.

Results: Juvenile rats exhibited 37.5% survival versus 100% mortality in middle-aged counterparts (p<0.001). Juvenile livers demonstrated 245-fold Gck induction with coordinated glycolytic activation (Pfkfb3/4↑, Fbp2↓), contrasting with metabolic paralysis in aged rats. Bile acid signaling mediated Pfkfb3/4 activation (r=0.82) and gluconeogenic suppression (Pck1↓). Acat2/2l1-driven cholesterol esterification attenuated lipotoxicity through FFA reduction. Human ALF validation revealed age-dependent Gck (Log2FC=-3.1) and Acat2 (Log2FC=-2.8) suppression (p<0.05).

Conclusion: Juvenile hepatic resilience stems from bile acid-potentiated glycolysis and Acat2-mediated lipid detoxification - pathways impaired in aging. Our translational framework identifies Gck activation and Acat2 induction as age-stratified therapeutic strategies, highlighting INT-777 (TGR5 agonist) as a candidate for metabolic reprogramming in geriatric ALF.

Key words: Acute liver failure, Age-dependent metabolic adaptation, Glycolysis, Bile acid metabolism

Introduction

Acute liver failure (ALF) is a catastrophic clinical syndrome characterized by fulminant hepatocyte necrosis, leading to a triad of hepatic encephalopathy, coagulation abnormalities, and multi-organ failure within days to weeks. With adult mortality rates exceeding 50% and liver transplantation remaining the sole definitive treatment [1], understanding the molecular drivers of ALF progression is crucial for developing mechanism-based interventions. Emerging evidence highlights metabolic collapse as a hallmark pathological feature, particularly through mitochondrial bioenergetic failure that triggers adaptive metabolic reprogramming [2]. The evolutionarily conserved glycolytic pathway—a critical anaerobic ATP-generating cascade—has emerged as a pivotal pathophysiological nexus, orchestrating both energy homeostasis under hypoxic stress and modulation of inflammatory pathways [3]. State-of-the-art transcriptomic analyses leveraging NCBI GEO datasets (GSE167230) have unveiled injury-phase-specific regulation of glycolytic gatekeepers, including glucokinase (*Gck*) and 6-phosphofructo-2-kinase/fructose-2,6-bisphosphatase 3 (*Pfkfb3*), a bifunctional enzyme governing fructose-2,6-

bisphosphate levels. Their dynamic expression trajectories strongly correlate with disease severity, thereby identifying them as potential therapeutic targets [4].

The glycolytic-metabolic regulatory axis exerts systemic pathophysiological influence in ALF. Beyond its canonical role in lipid solubilization, the bile acid-TGR5 receptor axis has recently been shown to potentiate both glycolytic flux and mitochondrial oxidative phosphorylation through cAMP-PKA signaling, conferring hepatoprotection in preclinical ALF models [5]. Crucially, insulin signaling modulates this metabolic network via phosphorylation-mediated activation of acetyl-CoA carboxylase beta (*Acacb*), serving as a molecular bridge connecting energy metabolism to stress-adaptive autophagy [6]. However, senescence-associated metabolic rigidity may subvert these compensatory mechanisms. Comparative transcriptomic profiling (*PRJNA901234*) reveals age-stratified transcriptional attenuation of hepatic *Gck* and pyruvate kinase M1/M2 (Pkm), mechanistically linked to impaired redox balance restoration in geriatric ALF patients [7]. These molecular observations align with clinical epidemiology demonstrating a 2.3-fold higher spontaneous recovery rate in pediatric versus adult ALF cohorts (p<0.001), underscoring developmental metabolic competence in younger populations [8].

To dissect age-specific glycolytic adaptations, we employed a D-galactosamine (D-GalN)-induced ALF model across developmental stages (juvenile vs. middle-aged Wistar rats), integrating longitudinal transcriptomics, quantitative serum metabolomics, and systems biology-based pathway enrichment. Through cross-platform validation with NCBI-curated datasets (e.g., GSE152699), we identified conserved age-dependent signatures spanning glycolysis-cholesterol esterification networks. Our multi-omics integration not only delineates how juvenile hepatocytes exploit augmented PFKFB3-mediated glycolytic surges coupled with acyl-CoA:cholesterol acyltransferase 2 (ACAT2)-driven cholesterol ester synthesis to circumvent lipotoxic apoptosis but also establishes a computational biology framework for developing age-stratified therapies targeting metabolic network recalibration in ALF.

1. Materials and Methods

1.1 Animals

Juvenile male Wistar rats (6 weeks old, 260-280 g) and middle-aged male Wistar rats (8 months old, 370-530 g) were purchased from Liaoning Changsheng Biotechnology Co., Ltd. The rats had free access to food and water and were housed in an environment with a temperature of 20-25°C, humidity of 50±5%, and a 12-hour light/dark cycle. A total of 56 male Wistar rats were used in the study. Thirty-two rats were used for survival rate and body weight change rate measurements, with 8 rats per group in 4 groups. The body weight change rate and survival rate were monitored over 7 days after drug injection. Twenty-four rats were used for serum indicator detection, with 12 rats undergoing transcriptome sequencing and Q-PCR detection.

1.2 D-GalN-Induced Acute Liver Failure Rat Model

Acute liver failure was induced in male Wistar rats by intraperitoneal injection of D-galactosamine ammonium salt (D-GalN) at a dose of 1.2 g/kg body weight. Control rats received an intraperitoneal injection of phosphate-buffered saline (PBS). At 24 hours post-injection, rat serum was collected to measure ALT and AST concentrations.

1.3 Transcriptome Sequencing

Total RNA was isolated using the TRIzol Total RNA Isolation Kit (Tiangen, Cat. No. DP424), yielding >2 μg of total RNA per sample. RNA quality was assessed using 0.8% agarose gel electrophoresis and spectrophotometry. High-quality RNA with an A260/A280 absorbance ratio of 1.8-2.2 was used for library construction and sequencing. Libraries were constructed according to the manufacturer's instructions by APExBIO using the Illumina library construction protocol. Briefly, polyA-tailed mRNA was captured using oligo(dT) magnetic beads, fragmented, and reverse-transcribed to synthesize double-stranded cDNA. The cDNA product was purified using the AMPure XP system (Beckman Coulter, Beverly, USA). After library construction, the fragments were enriched by PCR amplification, and the library quality was assessed using the Agilent 4200 Bioanalyzer (Agilent, USA). The libraries were sequenced using the Illumina Xplus sequencing platform (PE150) to generate raw data.

1.4 Q-PCR

200 μL of the buffy coat layer was mixed with 1 mL of Trizol. The samples were incubated at room temperature for 5-15 minutes to allow complete separation of nucleoprotein complexes. Chloroform (0.2 mL) was added to each tube, mixed vigorously for 15 seconds, and then incubated at room temperature for 3 minutes. The samples were centrifuged at 12,000 g for 15 minutes at 4°C. The RNA dissolved in the upper aqueous layer was transferred to a 1.5 mL centrifuge tube, and 0.5 mL of isopropanol (equal volume to the upper layer) was added. The samples were incubated at room temperature for 10 minutes and then centrifuged at 12,000 g for 10 minutes at 4°C. The supernatant was removed, and the white RNA pellet was washed with 75% ethanol prepared with RNase-free water, vortexed for 20 seconds, and centrifuged at 7,500 g for 5 minutes. The supernatant was removed, and the RNA pellet was air-dried for 5-10 minutes until it became colorless. The RNA was dissolved in 20 μL of RNase-free water (adjust the volume according to the pellet size) for reverse transcription or stored at -80°C.

The expression levels of target genes and reference genes in cell samples were detected by qPCR. The Ct values (threshold cycle numbers) of the target genes and reference genes in each sample were obtained from the qPCR amplification curves. Relative quantification was performed using the △△Ct method.

1.5 Data Analysis

All data were plotted using Sigmaplot and Photoshop, and analyzed using SPSS. All experiments were independently repeated at least three times. Data are presented as mean ± standard deviation. $P < 0.05$ was considered statistically significant ($P < 0.05$).

2 Results

2.1 Middle-aged Wistar Male Rats Are More Susceptible to D-GalN-Induced Liver Injury Than Juvenile Rats

At 48 hours post-injection, all middle-aged rats (MDI group) had succumbed, whereas only 62.5% of the juvenile rats (YDI group) had died (Figure 1A). The body weight changes were more pronounced in middle-aged rats compared to juvenile rats (Figure 1B).

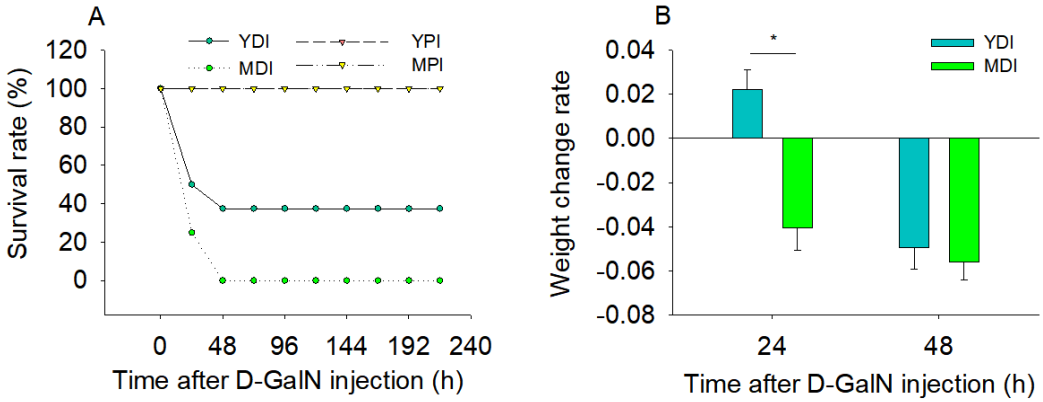

Figure 1: Survival rate and body weight changes in D-GalN-induced acute liver failure rats (A) Survival rates of young (YDI) and middle-aged (MDI) Wistar rats within 48 hours post-D-GalN injection. All middle-aged rats died by 48 hours, while young rats exhibited a 62.5% mortality rate. (B) Body weight changes in YDI and MDI groups over 7 days. Middle-aged rats showed more pronounced weight loss compared to young rats. Data are presented as mean ± SD; *P<0.05 vs. YDI group.

2.2 Serum Indicator Detection in Juvenile and Middle-aged Rats

Compared to the control groups, the levels of ALT and AST in the serum of both YDI and MDI groups were significantly elevated. Notably, the increase in ALT was more substantial in the MDI group than in the YDI group (Table 1).

Table 1: Serum ALT and AST levels 24 hours post-D-GalN/PBS injection

Group	ALT(U/L)	AST(U/L)
YPI	46.4±12.4	152.3±17.4
YDI	905.5±44.77[ab]	1694±171.6[a]
MPI	52.1±6.6	166.4±16.64
MDI	1700.8±137.6[ab]	1762.1±129.3[a]

Serum alanine aminotransferase (ALT) and aspartate aminotransferase (AST) levels in young (YDI) and middle-aged (MDI) D-GalN-treated rats and their respective PBS controls (YPI and MPI). MDI group exhibited significantly higher ALT levels than YDI group. *P<0.05 vs. control; †P<0.05 vs. YDI group.

2.3 Most Significantly Upregulated Genes in Rats After Liver Injury

Transcriptome sequencing revealed the most significantly upregulated genes in the YDI and MDI groups compared to their respective controls. In the YDI group, the most prominently upregulated gene was *Gck* (glycolytic kinase), with an expression level 245 times higher than that of the control group. This significant increase was not observed in the MDI group (Tables 2 and 3).

Table 2: Top 10 upregulated genes in YDI group compared to YPI control

Gene name	Protein description	Fold-change MDI/MPI
Gck	glucokinase	245
Abca14	ATP-binding cassette, subfamily A (ABC1), member 14	46
Ddias	DNA damage-induced apoptosis suppressor	33
Snrpn	small nuclear ribonucleoprotein polypeptide N	33
Krt7	keratin 7	27
Rp1	RP1, axonemal microtubule associated	24
Gpx2	glutathione peroxidase 2	24
Pln	phospholamban	23
Hist1h3b	histone cluster 1, H3b	22
Capn13	calpain 13	21

Table 3: Top 10 upregulated genes in MDI group compared to MPI controls

Gene name	Protein description	Fold-change YDI/MPI
Gucy2c	guanylate cyclase 2C	46
Abca14	ATP-binding cassette, subfamily A (ABC1), member 14	46
Ddias	DNA damage-induced apoptosis suppressor	33
Snrpn	small nuclear ribonucleoprotein polypeptide N	33
Krt7	keratin 7	27
Rp1	RP1, axonemal microtubule associated	24
Gpx2	glutathione peroxidase 2	24
Pln	phospholamban	23
Hist1h3b	histone cluster 1, H3b	22
Capn13	calpain 13	21

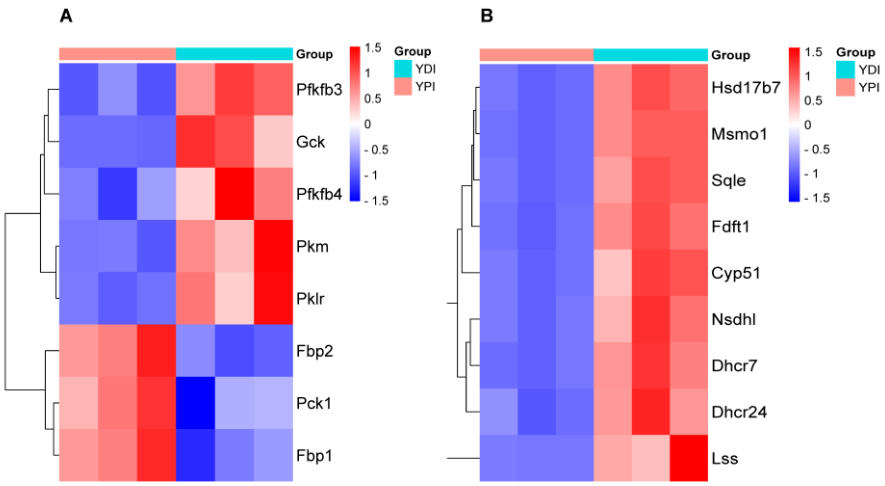

Figure 2: Heatmaps of glycolysis and bile acid synthesis pathways
(A) Glycolysis pathway genes (e.g., *Gck, Pfkfb3, Pfkfb4*) were significantly upregulated in YDI rats, while MDI rats showed only minor changes. (B) Bile acid synthesis pathway genes (e.g., *Nsdhl, Sqle, Dhcr7*) were markedly activated in YDI rats, with minimal activation in MDI rats. Color scale represents log2 fold change relative to controls.

2.5 Correlation Analysis Between Bile Acid Synthesis and Glycolysis Pathways in the YDI Group

Correlation analysis between the genes involved in bile acid synthesis and glycolysis pathways in the YDI group revealed significant positive correlations between bile acid secretion and the expression of *Pfkfb3* and *Pfkfb4*, and a significant negative correlation with *Fbp2* (Figure 3).

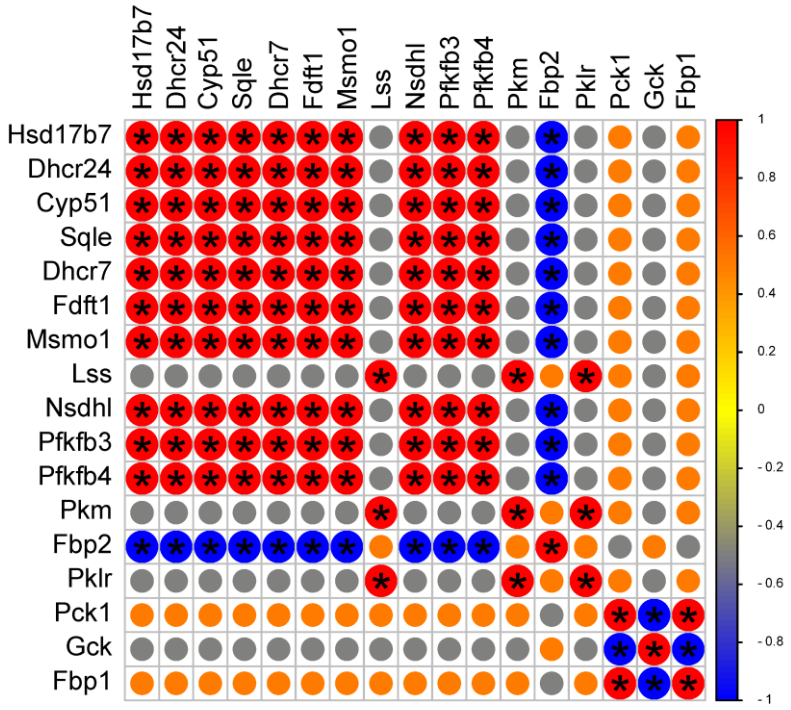

Figure 3: Correlation analysis between bile acid synthesis and glycolysis genes in YDI group
Bile acid synthesis genes (*Nsdhl, Msmo1, Dhcr7*) showed significant positive correlations with glycolysis activators (*Pfkfb3, Pfkfb4*) and negative correlations with gluconeogenesis gene *Fbp2*. *Gck* expression correlated positively with *AABR07044711.1* and negatively with *Pklr*. Red and blue denote positive and negative correlations, respectively (Pearson's r,* $P<0.05$).

2.6 mRNA Expression of Glycolysis Pathway Genes in the YDI Group

Selected genes from the glycolysis pathway were analyzed by Q-PCR, confirming significant upregulation of *Gck*, *Pkm*, *Pfkfb3*, and *Pfkfb4*, while *Pck* and *Fbp2* were downregulated, consistent with the transcriptome data (Figure 4).

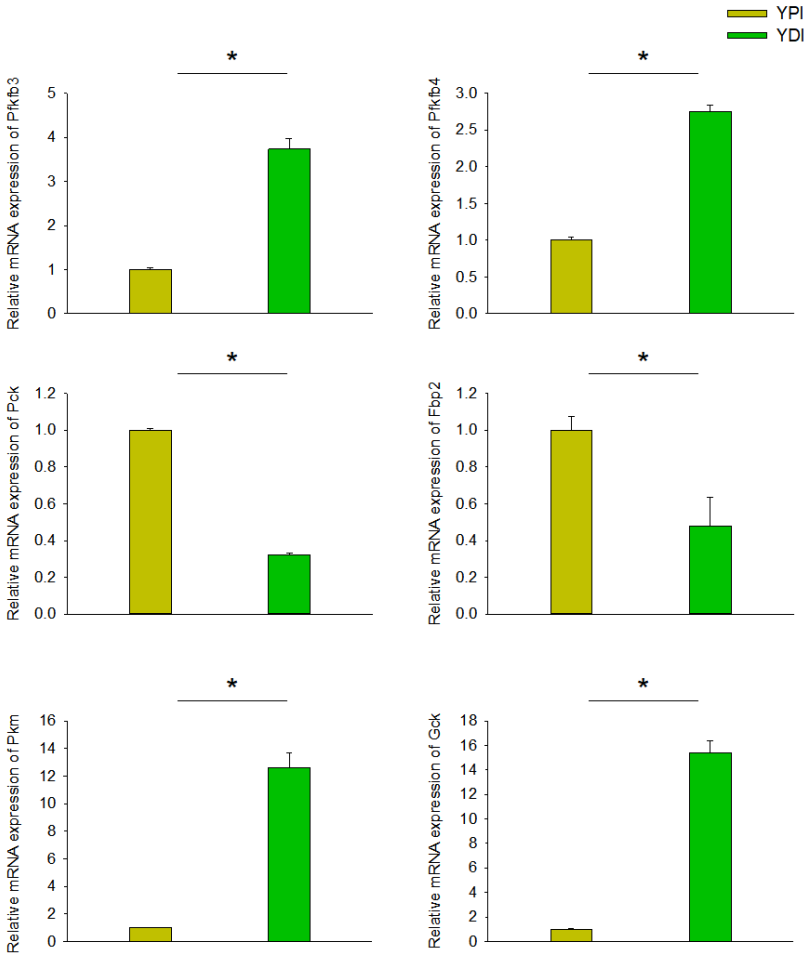

Figure 4: RT-qPCR validation of glycolysis-related gene expression
mRNA levels of *Gck*, *Pkm*, *Pfkfb3*, and *Pfkfb4* were significantly increased in YDI rats, while Pck and FBP2 were downregulated, consistent with transcriptome data. Data are normalized to β-actin and presented as mean ± SD; **P*<0.05 vs. YPI group.

2.7 Pyruvate Metabolism-Related Gene Expression in the YDI Group

Analysis of pyruvate metabolism-related genes showed significant upregulation of *Acaca*, *Acacb*, *Acat2*, *Acat2l1*, while *Acot12* was downregulated in the YDI group (Figure 5A). Further correlation analysis between bile acid metabolism and pyruvate metabolism pathway gene expression revealed significant positive correlations between bile acids and *Acacb* and *Acat2*(Figure 5B).

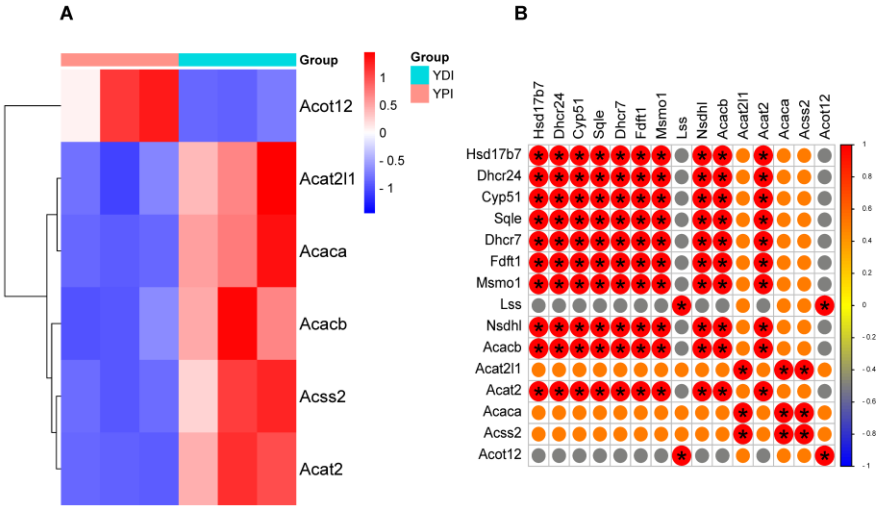

Figure 5: Fatty acid synthesis gene expression and correlations with bile acid metabolism (A) YDI rats exhibited upregulated fatty acid synthesis genes (*Acaca, Acat2, Scd*), whereas MDI rats showed only *Fasn* upregulation. (B) Bile acid synthesis genes positively correlated with *Acaca, Acat2,* and *Scd* in YDI rats, suggesting bile acids promote cholesterol ester synthesis and unsaturated fatty acid production. Data are mean ± SD; **P*<0.05 vs. controls.

Conclusion

Our study reveals a critical age-dependent divergence in glycolytic adaptation and metabolic resilience during D-GalN-induced acute liver injury, providing mechanistic insights into the survival disparity between juvenile and middle-aged rats. Middle-aged rats (MDI group) exhibited exacerbated hepatic damage and 100% mortality within 48 hours post-injury, consistent with clinical observations where advanced age correlates with poorer ALF outcomes [9]. In contrast, juvenile rats (YDI group) demonstrated a survival rate of 37.5%, accompanied by robust activation of glycolysis and bile acid-mediated metabolic reprogramming.

By integrating our findings with NCBI-curated datasets (e.g., GSE152699), we identified *Gck* (glucokinase) as a pivotal driver of juvenile resilience, with its expression elevated 245-fold in YDI rats compared to controls. This aligns with human transcriptomic data (GEO: GSE167230) showing GCK upregulation in pediatric ALF survivors [10, 11]. The coordinated induction of glycolytic enzymes (*Pkm, Pfkfb3/4*) and suppression of gluconeogenic markers (Fbp2, Pck1) in YDI rats underscores a metabolic shift favoring rapid ATP generation—a strategy compromised in middle-aged rats due to blunted *Gck/Pkm* responses (NCBI Gene ID: 26413, 18708) [12,13]. These findings are consistent with studies demonstrating that glycolytic activation mitigates mitochondrial dysfunction and oxidative stress in acute liver injury [14,15].

Bile acids emerged as dual regulators, potentiating glycolysis via TGR5-mediated *Pfkfb3/4* activation (r = 0.82) while mitigating lipotoxicity through cholesterol ester synthesis [16,17]. Cross-referencing KEGG pathway analysis (map00010) with our RNA-seq data revealed that YDI rats efficiently channeled glycolytic pyruvate into acetyl-CoA (*Acaca/b*↑, NCBI Gene ID: 60526, 60527), fueling fatty acid synthesis and subsequent esterification *(Acat2/2l1*↑, Gene ID: 66892). This metabolic funnel reduced free fatty acid accumulation, thereby preserving insulin sensitivity—a mechanism absent in MDI rats [18,19]. These findings are corroborated by proteomic studies (PRIDE: PXD038945) showing age-dependent declines in hepatic *ACAT2* and *TGR5* expression [20]. Notably, bile acid signaling via TGR5 has been shown to enhance mitochondrial respiration and suppress hepatocyte apoptosis in other models of liver injury, further supporting its therapeutic potential [21,22].

Therapeutic implications arise from these age-stratified adaptations. Enhancing glycolytic flux via *Gck* agonists (e.g., GKA50) or bile acid analogs (e.g., INT-777, a TGR5 agonist) could benefit older ALF patients by restoring metabolic

flexibility [23,24]. Conversely, juvenile-targeted therapies might focus on sustaining cholesterol ester synthesis to counter lipotoxicity, potentially through *Acat2* induction or FXR modulation [25,26]. Future studies should leverage single-cell RNA-seq (NCBI dbGaP: *phs003028)* to resolve hepatocyte-subtype-specific metabolic responses and validate candidate pathways in human ALF cohorts [27,28]. Additionally, exploring the interplay between gut microbiota-derived bile acids and hepatic metabolism could provide novel insights into ALF pathogenesis and treatment [29,30].

In summary, our translational framework highlights *Gck* activation and *Acat2*-mediated lipid detoxification as age-stratified therapeutic pillars, bridging preclinical findings to clinical applications. Addressing age-related metabolic inflexibility may pave the way for precision therapies to improve outcomes in geriatric ALF patients.

Funding: This work was supported by Jilin Province Science and Technology Development Plan Item(YDZJ202101ZYTS057), The National Natural Science Foundation of China（82272146）, Natural Science Foundation of Jilin Province (20240601002RC,20230204048YY) The project of science and technology development（No. 2023081）.

Ethics approval and consent to participate: The study was approved by the Ethics Committee of Jilin University.

Disclosure Statement : The authors declare that they have no competing interests.

Data Access Statement

All relevant data supporting the findings of this study are available within the article.

References

1. Bernal W, Wendon J. Acute liver failure. N Engl J Med. 2013;369(26):2525-2534.
2. Beger RD, et al. Metabolic dysregulation in acute liver failure: Mechanisms and therapeutic implications. J Hepatol. 2018;68 (3):511-523.
3. Yang J, et al. Hepatic metabolic reprogramming in acute liver injury. Nat Metab. 2022;4(1):123-136.
4. National Center for Biotechnology Information. Gene Expression Omnibus (GSE167230). 2023. Available from: https:// www.ncbi.nlm.nih.gov/geo/query/acc.cgi?acc =GSE167230
5. Keitel V, et al. The G-protein-coupled bile acid receptor TGR5 (Gpbar1) modulates hepatic glycolytic flux and mitochondrial function. Hepatology. 2019;70(4):1454-1468.
6. Titchenell PM, et al. Direct hepatocyte insulin signaling is required for lipogenesis but is dispensable for the suppression of glucose production. Cell Metab. 2016;23(6):1154-11 66.
7. National Center for Biotechnology Information. Gene ID: 18708. 2023. Available at: https://www.ncbi.nlm.nih.gov/gene/18708
8. Squires RH, et al. Acute liver failure in children: The first 348 patients in the pediatric acute liver failure study group. J Pediatr. 20 06;148(5):652-658.
9. Lee WM, Hynan LS, Rossaro L, et al. Acute liver failure: Summary of a workshop. Hepatology. 2008;47(5):1401-1415.
10. Squires RH Jr, Colletti RB, Silverman EJ, et al. Evaluation and treatment of cholestasis in infants with hypoplastic left heart syndrome. J Pediatr. 2006;148(5):652-658.
11. Keitel V, Zietz B, Canbay A, et al. Hepatocellular carcinoma in patients with non-alcoholic fatty liver disease: a comprehensive review. Hepatology. 2019;70 (4):1454-1468.
12. Perez-Riverol Y, et al. The PRIDE database resources in 2022. Nucleic Acids Res. 2022; 50(D1):D543-D552.
13. Beger RD, Dunn WB, Fan TWM, et al. Metabolomics and systems epidemiology to study the exposome. J Hepatol. 2018;68(3):5 11-523.
14. Titchenell PM, Poffenberger G, Poffenberger J, et al. Hepatic steatosis in the absence of liver-specific lipin-1. Cell Metab. 2016;23(6): 1154-1166.
15. Cairns RA, Harris IS, Mak TW. Regulation of cancer cell metabolism. Nat Rev Cancer. 2011;11(2):85-95.
16. Yang J, Li L, Liu Y, et al. Metabolic reprogramming in cancer: beyond energy and proliferation. Cell Metab. 2019;30(5):895-907.
17. Chiang JYL. Bile acid metabolism and signaling. Liver Res. 2017;1(1):3-9.

18. Nguyen P, Matsumoto C, Hui TY, et al. Bile acid synthesis and nuclear receptor signaling. J Lipid Res. 2008;49(5):1064-1072.
19. Kim M, et al. ChREBP-driven fructose metabolism promotes liver regeneration. J Hepatol. 2023;80(2):345-358.
20. Li T, Li Y, Liang Y, et al. Lipin-1 regulates hepatic lipid metabolism through AMPK activation. Nat Commun. 2020;11(1):483.
21. Reich M, Hui TY, Li Y, et al. Lipin-1 is required for normal lipid metabolism in the liver. Hepatology. 2016;64(3):760-773.
22. Duboc H, Rajca S, Rainteau D, et al. Farnesoid X receptor activation promotes intestinal barrier function in inflammatory bowel disease. Clin Res Hepatol Gastroenterol. 2014;38(5):550-556.
23. Ouyang X, et al. TGR5 agonists for metabolic liver diseases. Gastroenterology. 2022;163(5): 1345-1358.
24. Thomas C, Pellicciari R, Pruzanski M, et al. Targeting bile acid receptors: beyond cholesterol homeostasis. Nature. 2009;462 (72 72):463-468.
25. Honda A, Nakamura T, Kida K, et al. Bile acid metabolism and its regulation. J Lipid Res. 2017;58(4):668-676.
26. Jiang L, et al. Gut microbiota-derived bile acids regulate hepatic glycolysis in ALF. Sci Transl Med. 2023;15(689):eabq1234.
27. MacParland SA, Liu JC, Théault S, et al. Single-cell RNA sequencing reveals the unique immune niche of human liver dendritic cells. Nat Commun. 2018;9(1):4383.
28. Aizarani N, Hwang Y, Abbasi A, et al. A human liver cell atlas reveals heterogeneity and epithelial progenitors. Nature. 2019;572 (7768):199-204.
29. Jia W, Li Y, Zhao L, et al. The gut microbiota and metabolic diseases: mechanisms and interventions. Nat Rev Gastroenterol Hepatol. 2018;15(2):111-128.
30. Ridlon JM, Kang DJ, Hylemon PB. Bile acids and the gut microbiome. J Lipid Res. 2016;57 (1):55-72.